Inverse-time Backup Protection Based on Unified Characteristic Equation for Distribution Networks with High Proportion of Distributed Generations

Nana Chang, Guobing Song, *Senior Member*, *IEEE*, Zhongxue Chang, Yuping Zheng, and Xingang Yang

***Abstract*—The setting work of backup protection using steady-state current is tedious, and mismatches occasionally occur due to the increased proportion of distributed generations (DGs) connected to the power grid. Thus, there is a practical need to study a backup protection technology that does not require step-by-step setting and can be adaptively coordinated. This paper proposes an action sequence adaptive to fault positions that uses only positive sequence fault component (PSFC) voltage. Considering the influence of DGs, the unified time dial setting can be obtained by selecting specific points. The protection performance is improved by using the adjacent upstream and downstream protections to meet the coordination time interval in the case of metallic faults at the near- and far-ends of the line. Finally, the expression and implementation scheme for inverse-time backup protection (ITBP) based on the unified characteristic equation is given. Simulation results show that this scheme can adapt to DG penetration scenarios and can realize the adaptive coordination of multi-level relays.**

***Index Terms*—Inverse-time backup protection (ITBP), distributed generation (DG), positive sequence fault component (PSFC) voltage, unified characteristic equation, adaptive coordination.**

I. Introduction

As the grid structure becomes more complex and variable, the setting work of conventional non-unit backup protection based on delayed coordination is very tedious [1]. The increase of DG penetration and the flexible operation mode often lead to protection failures and malfunctions [2], [3]. At present, most wide-area backup protections (WABPs) require communication, and the cost and reliability of communication technology limit the application of WABPs [4]. Thus, there is a practical need to study backup protection technology that does not rely on communication.

Inverse-time overcurrent (ITOC) protections adjust the tripping time based on current measurement and can adapt to the fault severity [5]. Compared with traditional definite-time overcurrent protection, it can quickly eliminate faults near the power supply side [6]. ITOC protections are used in medium- and low-voltage distribution networks because of their economy and simplicity [7].

With a high proportion of DGs connected to the power grid, the traditional single-terminal radial distribution network becomes a complex multi-terminal power system. ITOC protection based on steady-state fault currents can hardly meet the requirements of selectivity and rapidity [8], [9]. Many methods to improve the coordination of ITOC protections have been proposed in the existing literature.

In [10]-[15], optimization algorithms such as genetic algorithms [10], particle swarm optimization algorithms [11], seeker optimization algorithms [12], linear programming [13], [14], and quadratic programming [15] were used to solve the coordination problem of protections. These algorithms optimized the inverse-time parameters and reduced the workload of step-by-step setting. They can greatly improve the selectivity and rapidity of protections, but so far there is no unified expression for the selection of the objective function.

In [16] and [17], the fault voltage was directly introduced as the third dimension of the traditional ITOC characteristic equation. Both [18] and [19] formed a new inverse-time characteristic equation directly using the fault voltage. The use of the fault voltage allows protections to satisfy the coordination relation, but the problem of heavy setting workload is not mentioned. Adaptive ITOC protections update relay settings online and can be used to solve the problem of difficulty in setting the relay values after DG penetration. However, there are problems with insufficient response time or dependence on communication [20].

The advantage of digital overcurrent relays (DORs) is programmable, so user-defined equations are widely used [21], [22]. The piece-wise linear characteristic was used in [22] to realize the coordination of DORs, thus maintaining a con-

Manuscript received: September 14, 2022; revised: February 26, 2023; accepted: June 2, 2023. Date of CrossCheck: June 2, 2023. Date of online publication: June 23, 2023.

This work was supported in part by the National Natural Science Foundation of China (NSFC-UKRI_EPSRC) (No. 52061635105) and in part by the Science and Technology Program of SGCC (No. 5100-202040327A-0-0-00).

N. Chang, G. Song (corresponding author), and Z. Chang are with the School of Electrical Engineering, Xi'an Jiaotong University, Xi'an, China (e-mail: changnna@163.com; song.gb@163.com; changzhx@163.com).

Y. Zheng is with State Key Laboratory of Smart Grid Protection and Control, NARI Group Corporation, Nanjing, China (e-mail: zhengyuping@sgepri. sgcc. com.cn).

X. Yang is with Electric Power Research Institute of State Grid Shanghai Electric Power Company, Shanghai, China (e-mail: xingangyang@163.com).

DOI: 10.35833/MPCE.2022.000591

stant time interval between the main/backup protection pairs. Furthermore, the fault component voltage was only present during the fault state and its distribution was characterized by the opposite of the fault voltage [23]. Therefore, it is of research value to use the fault component voltage to obtain a user-defined unified characteristic equation to implement the ITBP function.

The authors have proposed a fault identification method in [24], in which all protections used user-defined inverse-time equations, but the faulty line with the help of protection action signal (PAS) was needed to be identified. This paper aims to propose an ITBP scheme for distribution networks with high proportion of DGs. All protections adopt unified pickup value and time dial settings (TDSs), so the inverse-time characteristic parameters do not need to be set step-by-step. It uses only the PSFC voltages to realize the action sequence adaptive to fault positions. The tripping time is set adaptively according to current fault conditions.

The remainder of this paper is organized as follows. The distribution pattern of the PSFC voltage and the effect of the DG penetration on its amplitude are analyzed in Section II. Section III gives the ITBP scheme based on unified characteristic equations. The implementation of the ITBP scheme is given in Section IV. Section V carries out simulations in different scenarios for validation. Finally, conclusions are given in Section VI.

II. Distribution Pattern of PSFC Voltage and Effect of DG Penetration on Its Amplitude

A. Equivalent Circuit of DGs

DGs are divided into rotating-type distributed generations (RTDGs) and inverter-interfaced distributed generations (IIDGs) according to different grid connection modes.

RTDGs are similar to conventional generators and are analyzed using the Thevenin equivalent model [25]. They can provide short-circuit currents to the network after a fault.

IIDGs include permanent-magnet synchronous generator (PMSG) based wind turbines, photovoltaic (PV) generators, etc. They must have low voltage ride-through (LVRT) capability, giving priority to reactive power delivery to the grid in the event of a system fault. Referring to GB_T 19963.1-2021 [26], the control strategy used by PMSGs in this paper is shown as:

$$i_{d\mathrm{ref}}=\min\left\{\frac{P_{\mathrm{ref}}}{U_{\mathrm{PCC},f}},\sqrt{I_{\max}^2-i_{q\mathrm{ref}}^2}\right\} \tag{1}$$

$$i_{q\mathrm{ref}}=\begin{cases}1.5\cdot(0.9-\gamma)I_{\mathrm{N}} & 0.2\le\gamma\le 0.9\\ 1.05I_{\mathrm{N}} & \gamma<0.2\end{cases} \tag{2}$$

where $i_{d\mathrm{ref}}$ and $i_{q\mathrm{ref}}$ are the active and the reactive current references, respectively; P_{ref} is the active power reference; $U_{\mathrm{PCC},f}$ is the grid voltage at the point of common coupling (PCC); $\gamma=U_{\mathrm{PCC},f}/U_{\mathrm{N}}$, and U_{N} is the rated voltage; I_{N} is the rated current; and $I_{\max}$ is the maximum fault current output of the DG.

The control strategy used by PV generators is shown in (1) and (3) [27].

$$i_{q\mathrm{ref}}=\begin{cases}2\cdot(1-\gamma)I_{\mathrm{N}} & 0.5\le\gamma\le 0.9\\ I_{\mathrm{N}} & \gamma<0.5\end{cases} \tag{3}$$

The fault current i_{DG} of IIDGs is:

$$i_{\mathrm{DG}}=\sqrt{i_{d\mathrm{ref}}^2+i_{q\mathrm{ref}}^2}\angle\arctan\frac{i_{q\mathrm{ref}}}{i_{d\mathrm{ref}}} \tag{4}$$

Thus, from (4), the maximum angle $\varphi_{\max}$ of i_{DG} lagging $U_{\mathrm{PCC},f}$ occurs at $\gamma=0.2$, which is:

$$\varphi_{\max}=\begin{cases}\arctan\dfrac{1.05I_{\mathrm{N}}}{\sqrt{I_{\max}^2-(1.05I_{\mathrm{N}})^2}} & \text{PMSGs}\\ \arctan\dfrac{I_{\mathrm{N}}}{\sqrt{I_{\max}^2-I_{\mathrm{N}}^2}} & \text{PV generators}\end{cases} \tag{5}$$

For the PMSG, $\varphi_{\max}=31.67°$ when $I_{\max}=2I_{\mathrm{N}}$ and $\varphi_{\max}=61.05°$ when $I_{\max}=1.2I_{\mathrm{N}}$. Considering the current limit of the PV inverter, taking $I_{\max}=1.1I_{\mathrm{N}}$, we can obtain $\varphi_{\max}=78.14°$.

The fault current of the IIDG is mainly determined by the control strategy. However, its transient process is very short and does not affect the fault steady-state output current [28], [29]. So, the IIDG can be equivalent to a constant current source at the corresponding voltage $U_{\mathrm{PCC},f}$ in the case of grid faults [29].

This paper mainly focuses on the influence of DG output characteristics on the additional network of PSFC. Therefore, the dashed box in Fig. 1 is used to represent the equivalent circuit of IIDGs in the additional network of PSFC. When the green dashed line in the dashed box is deleted, it represents the equivalent circuit of RTDGs.

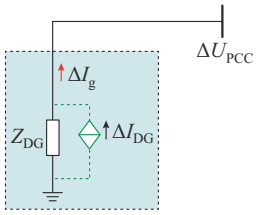

Fig. 1. Equivalent circuit of DGs in additional network of PSFC.

In Fig. 1, Z_{DG} is the equivalent impedance; ΔI_{DG} is the PSFC current without a current limiting strategy; ΔI_{g} is the PSFC current supplied to the grid by DG; and ΔU_{PCC} is the PSFC voltage at PCC.

B. Distribution Pattern of PSFC Voltages

Figure 2 shows a single-ended radial network containing grid-connected *PQ* controlled DGs. S represents the system source; R_1-R_3 represent the relays; Ld_1-Ld_4 represent the loads; f_1-f_3 represent the fault points at the near-end of Line1-Line3, respectively; A, B, C, and D represent bus numbers; and *f* represents a fault point on Line3.

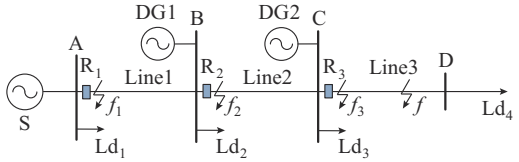

Fig. 2. Single-ended radial network containing grid-connected *PQ* controlled DGs.

Figure 3 gives the additional network of PSFC when a three-phase short-circuit fault occurs at f. ΔI_{s1} and Z_{s1} are the PSFC current and equivalent positive sequence impedance (PSI) of S, respectively; ΔI_{g1} and ΔI_{g2} are the PSFC currents supplied by DG_1 and DG_2, respectively; Z_{DG1} and Z_{DG2} are the equivalent PSI of DG_1 and DG_2, respectively; ΔI_{DG1} and ΔI_{DG2} are the PSFC currents supplied by DG_1 and DG_2 without a current limiting strategy, respectively; z_1 is the PSI per unit length; L_1 and L_2 are the lengths of Line1 and Line2, respectively; x is the length from bus C; ΔI_{1j} and ΔU_{1j} are the PSFC current and voltage of R_j, respectively; ΔI_{L11} - ΔI_{L13} and Z_{L11} - Z_{L13} are the PSFC currents and PSI for Ld_1-Ld_3, respectively; Z_{feq} is the equivalent PSI to the right of f; and $-U_{x|0|}$ is the pre-fault voltage of f. The reference direction is from the bus to the line.

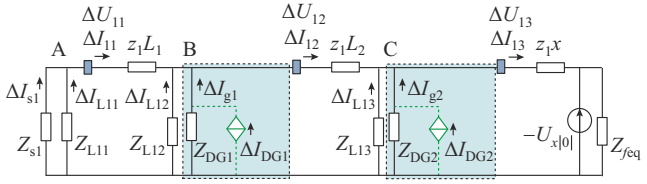

Fig. 3. Additional network of PSFC.

When a fault occurs, the voltage on each bus decreases while the equivalent impedance of the load remains constant. This results in a reduction in the fault current flowing through the load, which causes its PSFC current to flow from the line to the bus [30]. From (5) and Fig. 1, it can be observed that ΔI_{g1} lags ΔU_{11} and ΔI_{g2} lags ΔU_{12} at an angle of [0°, 180°] in the reference direction, so the PSFC current of IIDG flows from line to bus. Therefore, the PSFC current directions of DG_1, DG_2, and the loads are in the opposite direction to that specified.

According to Kirchhoff's current law, the PSFC currents flowing through the relays are in the specified direction. According to circuit theory, the PSFC voltage of each relay is:

$$\begin{cases} \Delta U_{13} = -U_{x|0|} + z_1 x \Delta I_{13} \\ \Delta U_{12} = \Delta U_{13} + z_1 L_2 \Delta I_{12} \\ \Delta U_{11} = \Delta U_{12} + z_1 L_1 \Delta I_{11} \end{cases} \tag{6}$$

ΔI_{13}, ΔI_{12}, and ΔI_{11} are all in the same direction as the reference, so $z_1 x \Delta I_{13}$, $z_1 L_2 \Delta I_{12}$, and $z_1 L_1 \Delta I_{11}$ are all positive values, while $-U_{x|0|}$ is negative. Therefore, the voltage drop on each line makes the PSFC voltage satisfy the relationship of (7).

$$|\Delta U_{13}| > |\Delta U_{12}| > |\Delta U_{11}| \tag{7}$$

Figure 4 shows the distribution patterns of PSFC voltages for R_1-R_3, whose amplitudes are inversely proportional to the fault position. The closer to the fault point, the greater the PSFC voltage value.

C. Effect of DG Penetration on PSFC Voltage Amplitude

The PSFC voltage is obtained by subtracting the pre-fault voltage from the fault voltage, and its amplitude is determined by the pre-fault voltage and the fault position when a fault occurs. DG penetration will support the grid voltage, the strength of which is related to DG connection location and capacity [31]. The larger the DG connection capacity is, the stronger the support and the larger the pre-fault voltage are.

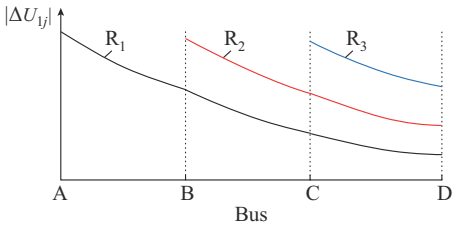

Fig. 4. Distribution patterns of PSFC voltages for R_1-R_3.

The change in DG connection capacity is achieved by changing the number of DGs in Fig. 2. Let the number of DG_1 connected to bus B be m and the number of DG_2 connected to bus C be n. Formula (6) shows that the PSFC voltages of R_1-R_3 still satisfy the relationship of (7) when the DG connection capacity is changed.

To achieve a unified characteristic equation, the adjacent protections should meet the selectivity requirement for any fault position. Combined with Fig. 4, it can be observed that f_3 is the most severe fault position when a metallic fault occurs. At this point, the PSFC voltages of R_3 and R_2 and the difference ΔU_{R23} between R_3 and R_2 are:

$$\begin{cases} \Delta U_{13} = -U_{x|0|} \\ \Delta U_{12} = -U_{x|0|} + z_1 L_2 (\Delta I_{11} + \Delta I_{L12} + m\Delta I_{g1}) \\ \Delta U_{R23} = z_1 L_2 \Delta I_{12} = z_1 L_2 (\Delta I_{11} + \Delta I_{L12} + m\Delta I_{g1}) \end{cases} \tag{8}$$

Figure 5 shows the PSFC voltage amplitude distribution after DG penetration when the fault occurs at f_3.

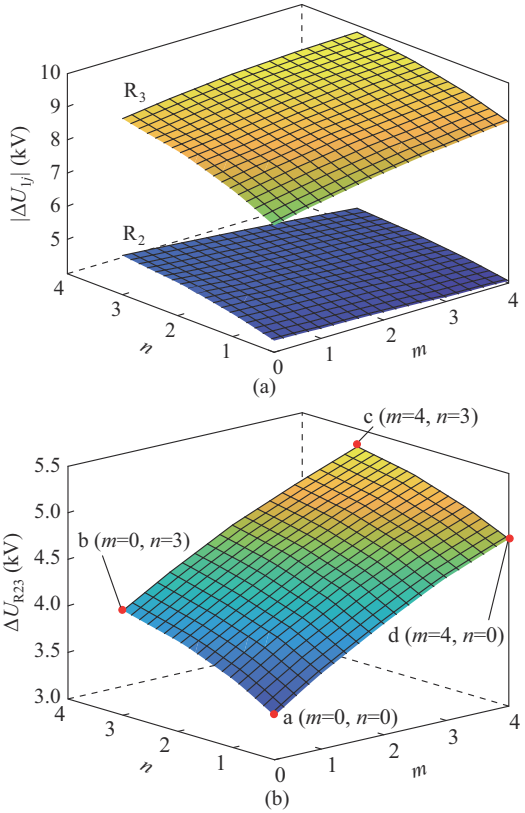

Fig. 5. PSFC voltage amplitude distribution after DG penetration. (a) PSFC voltage of R_3 and R_2. (b) ΔU_{R23}.

It can be observed from Fig. 5(a) that DG penetration does not change the distribution pattern of the PSFC voltage, but its connection location and capacity affect the PSFC voltage amplitude. The amplitude of ΔU_{13} depends on $U_{x|0|}$, which is mainly supported by DG and increases with m and n. The amplitude of ΔU_{12} is determined by both $U_{x|0|}$ and $m\Delta I_{g1}$. Figure 5(b) shows that ΔU_{R23} is jointly determined by m and n. a, b, c, and d indicate the different states of DG_1 and DG_2, where a ($m=0$, $n=0$) indicates that both DG_1 and DG_2 are out of operation; b ($m=0$, $n=3$) indicates that DG_1 is out of operation and DG_2 is operating at the maximum capacity; c ($m=4$, $n=3$) indicates that both DG_1 and DG_2 are operating at the maximum capacity; and d ($m=4$, $n=0$) indicates that DG_1 is operating at the maximum capacity and DG_2 is out of operation.

To sum up, the PSFC voltage still has a natural distribution pattern after the DG is connected to the grid. The PSFC voltage of different relays is different, and its natural distribution pattern can reflect the fault severity detected by each relay, which provides a theoretical basis for implementing the ITBP scheme based on unified inverse-time equation.

III. ITBP Scheme Based on Unified Characteristic Equation

A. Characteristic Equation and Parameter Selection Principle

1) Characteristic Equation

The ITOC characteristic equation specified by the International Electrotechnical Commission (IEC) is shown in (9) [32].

$$t_j = \frac{A \cdot TDS_j}{(I_j/I_{pj})^{\alpha} - 1} \tag{9}$$

where t_j, TDS_j, I_j, and I_{pj} are the tripping time, time dial setting, measured current, and pickup current of R_j, respectively; and A and α are the characteristic parameters, which are set to be 0.14 and 0.02, respectively, when using the standard inverse (SI) curve.

To ensure adaptive coordination of multi-level relays, the relay action time needs to be determined according to the ladder-type principle. Therefore, the characteristic parameters TDS_j and I_{pj} in (9) need to be set step-by-step starting from the relay farthest from the power source [22].

Compared with the conventional ITOC characteristic equation, the ITBP scheme uses the PSFC voltage instead of the fault current. The unified characteristic equation for the whole network when using SI curve is:

$$t_j = \frac{0.14 \cdot TDS}{(\left|\Delta U_{1j}\right| / \Delta U_p)^{0.02} - 1} \tag{10}$$

where ΔU_p is the pickup value of the PSFC voltage; and *TDS* is the unified time dial setting.

When $\left|\Delta U_{1j}\right| > \Delta U_p$, (10) starts and calculates t_j. When $\left|\Delta U_{1j}\right| < \Delta U_p$, (10) does not start.

2) Selection Principle of TDS

The ITBP scheme that has not been set step-by-step uses a unified *TDS*. For any fixed topology network, to realize the absolute selectivity between adjacent upstream and downstream protections, the value of *TDS* shall meet the following two conditions.

1) When used as the local backup protection of the line, the tripping time should be greater than that of time-limited instantaneous overcurrent protection, which is taken as 0.5 s in this paper. Therefore, there exists:

$$0.5 \le \frac{0.14 \cdot TDS}{(\Delta U_j^*)^{0.02} - 1} \tag{11}$$

where $\Delta U_j^* = \left|\Delta U_{1j}\right| / \Delta U_p$.

Formula (12) can be obtained by transforming (11).

$$TDS \ge \frac{0.5((\Delta U_j^*)^{0.02} - 1)}{0.14} \tag{12}$$

2) The tripping time difference between adjacent protections must be greater than the coordination time interval (CTI). For R_j and adjacent upstream R_{j-1}, there exists:

$$\frac{0.14 \cdot TDS}{(\Delta U_{j-1}^*)^{0.02} - 1} - \frac{0.14 \cdot TDS}{(\Delta U_j^*)^{0.02} - 1} \ge CTI \tag{13}$$

Formula (14) can be obtained by transforming (13).

$$TDS \ge \frac{CTI}{0.14 \cdot [1/((\Delta U_{j-1}^*)^{0.02} - 1) - 1/((\Delta U_j^*)^{0.02} - 1)]} \tag{14}$$

In summary, to ensure both selectivity and rapidity, the *TDS* should take the larger one of (12) and (14) when both of them are equations. Therefore, the selection principle of *TDS* can be expressed as:

$$TDS = \max\left\{\frac{0.5((\Delta U_j^*)^{0.02} - 1)}{0.14}, \frac{CTI}{0.14 \cdot [1/(\Delta U_{j-1}^*)^{0.02} - 1) - 1/((\Delta U_j^*)^{0.02} - 1)]}\right\} \tag{15}$$

For the first part of (15), the value of *TDS* is directly proportional to the PSFC voltage. When there is no DG connection, it only needs to ensure that this part is satisfied when a metallic short-circuit fault occurs at f_1. When the capacities of DG_1 and DG_2 are the largest, affected by their supporting effect, it is necessary to ensure that this part is satisfied when a metallic short-circuit fault occurs at f_3. The *TDS* obtained in this case is recorded as TDS_1.

For the second part of (15), the value of *TDS* is determined by the PSFC voltage amplitude of adjacent protections and their difference. The time difference of adjacent protections in the case of near-end faults is smaller than that of far-end faults. Therefore, this part should consider a three-phase fault occurring at f_2 and f_3. With faults occurring at f_3, the time-PSFC voltage curves obtained at a-d are shown in Fig. 6.

As shown in Fig. 6, the maximum *TDS* (TDS_{max}) is taken at b ($m=0$, $n=3$). According to Fig. 5, at b, the PSFC voltages of R_2 and R_3 are larger, but the voltage difference is smaller, which leads to the maximum *TDS* in the four scenarios. Therefore, when DG_2 connected to the downstream bus operates at the maximum capacity and DG_1 connected to the adjacent upstream bus exits, the *TDS* value satisfying the second part of (15) is calculated.

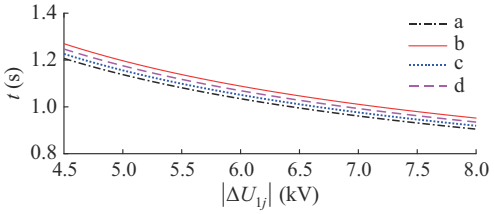

Fig. 6. Time-PSFC voltage curves obtained at a-d.

Calculate all *TDS* values when the fault occurs at f_1, f_2, and f_3, and take TDS_{max} as the unified *TDS* of the whole network.

3) Selection Principle of ΔU_p

The ITBP scheme that has not been set step-by-step uses a unified pickup setting. The voltage deviation for three-phase supplies up to 20 kV is ±7% of U_N [24]. To avoid voltage fluctuations caused by system disturbances and load switching that may lead to false activation of the protection, ΔU_p is taken as:

$$\Delta U_p = 1.1 \cdot 0.07 U_N \tag{16}$$

B. Improved Scheme Based on Unified Characteristic Equation

TDS_{max} ensures that all protections meet selectivity, but the rapidity, especially that of remote backup protections, is challenging to meet. Therefore, this paper intends to improve the ITBP performance through the ideal tripping time when all protections meet CTI requirements in the case of three-phase metallic faults at the near- and far-ends of the line.

With faults occurring at the near- or far-end of the line, the tripping time of all relays before and after performance improvement are shown in Table I.

TABLE I
TRIPPING TIME OF ALL RELAYS BEFORE AND AFTER PERFORMANCE IMPROVEMENT

Fault position	Relay	PSFC voltage	Tripping time calculated by (10)	Ideal tripping time
At near-end of Line3	R_3	$\lvert\Delta U_{13n}\rvert$	t_{3n}	t_{3n}
	R_2	$\lvert\Delta U_{12n}\rvert$	t_{2n}	t_{2n}
	R_1	$\lvert\Delta U_{11n}\rvert$	t_{1n}	$t_{2n}+CTI$
At far-end of Line3	R_3	$\lvert\Delta U_{13r}\rvert$	t_{3r}	t_{3r}
	R_2	$\lvert\Delta U_{12r}\rvert$	t_{2r}	$t_{3r}+CTI$
	R_1	$\lvert\Delta U_{11r}\rvert$	t_{1r}	$t_{3r}+2\cdot CTI$
At near-end of Line2	R_2	$\lvert\Delta U'_{12n}\rvert$	t'_{2n}	t'_{2n}
	R_1	$\lvert\Delta U'_{11n}\rvert$	t'_{1n}	t'_{1n}
At far-end of Line2	R_2	$\lvert\Delta U'_{12r}\rvert$	t'_{2r}	t'_{2r}
	R_1	$\lvert\Delta U'_{11r}\rvert$	t'_{1r}	$t'_{2r}+CTI$

Considering the programmability of DORs, $y=kx+b$ is used to accelerate the remote backup protection. The function of backup relay i corresponding to main relay j is t_{ij}. Its parameters k_{ij} and b_{ij} are obtained from PSFC voltage and ideal tripping time in the cases of near- and far-ends faults, as shown in Table II.

TABLE II
PARAMETER VALUES OF $y=kx+b$

Function	Parameter value	
	k_{ij}	b_{ij}
t_{23}	$(t_{3r}+CTI-t_{2n})/(\lvert\Delta U_{12r}\rvert-\lvert\Delta U_{12n}\rvert)$	$t_{2n}-k_{23}\lvert\Delta U_{12n}\rvert$
t_{13}	$(t_{3r}+CTI-t_{2n})/(\lvert\Delta U_{11r}\rvert-\lvert\Delta U_{11n}\rvert)$	$t_{2n}+CTI-k_{13}\lvert\Delta U_{11n}\rvert$
t_{12}	$(t'_{2r}+CTI-t'_{1n})/(\lvert\Delta U'_{11r}\rvert-\lvert\Delta U'_{11n}\rvert)$	$t'_{1n}-k_{12}\lvert\Delta U'_{11n}\rvert$

When the fault point moves from the near-end to the far-end, the farther the line is from the fault point, the smaller the variation range of the PSFC voltages. Thus, the PSFC voltage variation range of t_{13} is smaller than that of t_{23} and t_{12}. It can be inferred from Table I that $t_{3r}<t_{2n}=t'_{2r}<t'_{1n}$ and $t_{3r}-t_{2n}<0<t'_{1n}-t'_{2r}$. Then, the tripping time variation range $t_{3r}+CTI-t_{2n}$ of t_{23} and t_{13} is greater than the tripping time variation range $t'_{2r}+CTI-t'_{1n}$ of t_{12}. Therefore, the absolute value $\lvert k_{13}\rvert$ is greater than $\lvert k_{23}\rvert$ or $\lvert k_{12}\rvert$, and t_{13} is used to obtain the ITBP scheme with improved protection performance.

Figure 7 shows the implementation process of the unified characteristic equation. The black dotted line is the ITBP tripping curve obtained by TDS_{max}, and the blue dotted line is the tripping curve obtained by TDS_1. The green and magenta dotted lines are the tripping curves of R_2 and R_1, respectively, after performance improvement. The red solid line is the proposed ITBP tripping curve based on nonstandard inverse-time characteristics. Point h is the intersection of the extension line of t_{13} and the blue dotted line, and its corresponding PSFC voltage is $\lvert\Delta U_{1h}\rvert$.

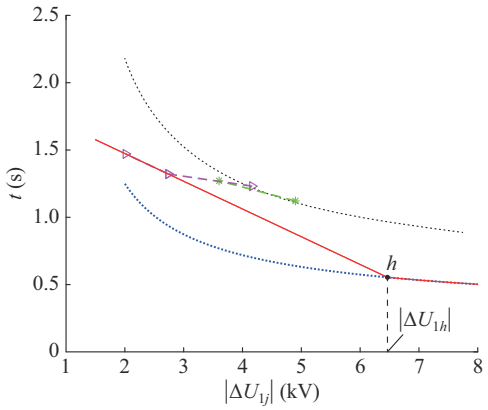

Fig. 7. Implementation process of unified characteristic equation.

When t_{13} is used as the ITBP tripping curve for all relays, due to the increase in the curve slope at the most serious fault, the time difference of adjacent protections will be greater than that of the original tripping curve, which improves the protection selectivity. Since t_{13} is below the black dotted line, the tripping time of all relays will be reduced, which improves the protection rapidity. When t_{13} is under the blue dotted line, the blue dotted line is used to realize the backup protection function.

The tripping time of relay depends on the PSFC voltage amplitude, and its values are different under different fault types. When a phase-to-phase fault (PPF) or a phase-to-phase-to-ground fault (PPGF) occurs at point *f*, the sum of the PSFC voltage and the negative sequence fault component (NSFC) voltage at point *f* is known from the composite sequence network to be equal to the PSFC voltage of the three-phase fault [33]. From the boundary conditions at the fault point, there exists:

$$\left|\Delta U_{1\mathrm{f}}\right| + \left|\Delta U_{2\mathrm{f}}\right| = U_{x|0|} \tag{17}$$

where $\Delta U_{1\mathrm{f}}$ and $\Delta U_{2\mathrm{f}}$ are the PSFC voltage and NSFC voltage, respectively.

The additional network of the PSFC to the left of the fault point is similar for different fault types. Therefore, a fault type factor λ_j is introduced in this paper, which is used to reduce the effect of the fault type on the PSFC voltage amplitude [24], which can be expressed as:

$$\lambda_j = \frac{\left|\Delta U_{1j}\right| + \left|\Delta U_{2j}\right|}{\left|\Delta U_{1j}\right|} \tag{18}$$

Therefore, the following PSFC voltages are revised by λ_j. The final characteristic equation is:

$$t_j = \begin{cases} k_{13}\left|\Delta U'_{1j}\right| + b_{13} & \left|\Delta U'_{1j}\right| \le \left|\Delta U_{1h}\right| \\ \dfrac{0.14 \cdot TDS_1}{(\Delta U_j'^{*})^{0.02} - 1} & \left|\Delta U'_{1j}\right| > \left|\Delta U_{1h}\right| \end{cases} \tag{19}$$

where $\left|\Delta U'_{1j}\right| = \lambda_j \left|\Delta U_{1j}\right|$.

The parameters in (19) are obtained offline by setting DG state and selecting specific fault points when a three-phase metallic fault occurs. The tripping time automatically obtains the coordination relationships of all protections, so the ITBP scheme is adaptive.

IV. Implementation of ITBP Scheme

The ITBP scheme is positioned as a local backup of the time-limited current protection for that line and a remote backup for the adjacent downstream line [34]. As it implements the backup protection function, the set value I_{set} of the existing adaptive definite-time overcurrent protection is used as an auxiliary criterion to determine whether a fault exists within its corresponding delay time $t_{j,\mathrm{delay}}$ [34]. The flowchart of the proposed scheme is shown in Fig. 8.

The proposed scheme can protect the whole line and automatically identify the faults at the far-end of this line and the near-end of adjacent lines. It has the advantages of not setting the inverse-time characteristic parameters step-by-step and adaptively setting the tripping time.

V. Simulation Results

A. Simulation Model

Numerous simulation tests have been carried out to verify the correctness of ITBP in action sequence. The simulation model of a radial network shown in Fig. 9 is established in PSCAD/EMTDC.

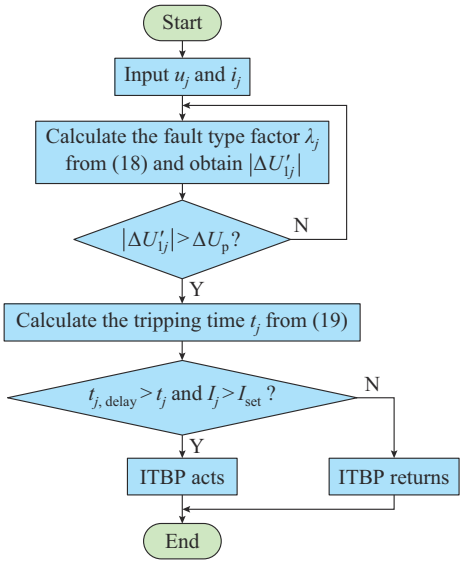

Fig. 8. Flowchart of proposed scheme.

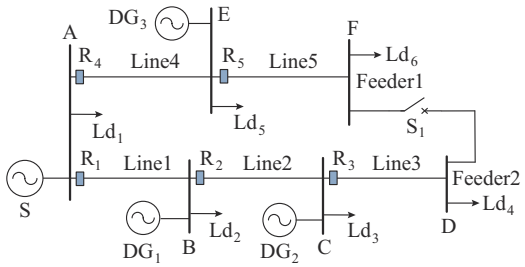

Fig. 9. Simulation model of radial network.

The active distribution network contains two feeders and three DGs, and the rated voltage of the system is 10 kV. S_1 is a tie switch, which is open during normal operation. The lumped parameter model is adopted and the length of all lines is 5 km. The positive sequence resistance and reactance of the line are 0.27 Ω/km and 0.352 Ω/km, respectively. The capacity of Ld_1-Ld_4 is (1+j0.1)MVA, and the capacity of Ld_5 and Ld_6 is (2+j0.5)MVA. DG_1 and DG_2 are PV generators with a rated capacity of 4 MVA and $I_{\mathrm{max,PV}} = 1.1 I_{\mathrm{N,PV}}$, where $I_{\mathrm{max,PV}}$ and $I_{\mathrm{N,PV}}$ are the maximum fault current output and rated current of the PV generator, respectively. DG_3 is PMSG with a rated capacity of 3 MVA and $I_{\mathrm{max,PMSG}} = 1.5 I_{\mathrm{N,PMSG}}$, where $I_{\mathrm{max,PMSG}}$ and $I_{\mathrm{N,PMSG}}$ are the maximum fault current output and rated current of the PMSG, respectively. The sampling frequency and CTI are taken to be 2 kHz and 0.2 s, respectively.

B. Simulation Verification of ITBP Scheme

Table III lists the *TDS* and TDS_1 values in the case of the near-end fault of each line when DGs are connected. Table IV lists the *TDS* values with faults under different fault positions and DG statuses. DG connection represents that DG operates at the maximum capacity.

When the minimum accuracy of *TDS* is set to be 0.01, $TDS_1 = 0.18$ and $TDS_{\max} = 0.36$. Comparing the *TDS* values obtained at the near-end of Line2 and Line5, it can be observed that the supporting effect of DG significantly increases the *TDS* value.

TABLE III
TDS AND TDS_1 VALUES IN CASE OF NEAR-END FAULT OF EACH LINE

Fault position	PSFC voltage (kV)	*TDS*	TDS_1
Near-end of Line1/Line4	$\lvert\Delta U_{11}\rvert = 8.338$	0.174	0.18
Near-end of Line2	$\lvert\Delta U_{12}\rvert = 8.789$	0.178	
Near-end of Line3	$\lvert\Delta U_{13}\rvert = 8.969$	0.180	
Near-end of Line5	$\lvert\Delta U_{15}\rvert = 8.365$	0.175	

TABLE IV
TDS VALUES UNDER DIFFERENT FAULT POSITIONS AND DG STATUSES

Fault position	DG status			*TDS*
	DG_1	DG_2	DG_3	
Near-end of Line2	Connection	Connection	Exit	0.218
	Exit			0.209
	Connection	Connection	Connection	0.211
	Exit			0.199
Near-end of Line3	Connection	Connection	Exit	0.331
		Exit		0.301
	Exit	Connection		0.355
		Exit		0.318
	Connection	Connection	Connection	0.308
		Exit		0.275
	Exit	Connection		0.332
		Exit		0.292
Near-end of Line5	Connection	Connection	Connection	0.184
			Exit	0.171

With faults occurring at the near- and far-ends of Line2 and Line3, the first-order function after performance improvement can be expressed as:

$$\begin{cases} t_{12} = -0.049\lvert\Delta U_{11}\rvert + 1.505 \\ t_{13} = -0.167\lvert\Delta U_{11}\rvert + 1.963 \\ t_{23} = -0.092\lvert\Delta U_{12}\rvert + 1.758 \end{cases} \tag{20}$$

The characteristic equation of the ITBP scheme is:

$$t = \begin{cases} -0.167\lvert\Delta U_1'\rvert + 1.963 & \lvert\Delta U_1'\rvert \le 8.721 \\ \dfrac{0.14 \cdot 0.18}{(\Delta U_j^*)^{0.02} - 1} & \lvert\Delta U_1'\rvert > 8.721 \end{cases} \tag{21}$$

Table V shows the ITBP operation behaviors of the Feeder2 at different fault positions when DG_1 and DG_2 are connected and DG_3 exits.

Figure 10 shows the time-position coordination relationship of all relays obtained from Table V, where L is the total length of Line1-Line3. The tripping curves illustrate that the proposed scheme automatically reflects the correlation between each relay and fault position.

The adaptation of the proposed scheme to different fault types and feeders when DG_1 and DG_2 are connected and DG_3 exits is shown in Fig. 11. As can be observed from Fig. 11, the tripping time of R_2 and R_3 is basically the same for different fault types, as is the tripping time for R_4 and R_5. According to the comparison between Fig. 11(a) and (b), due to the influence of DG penetration, the supporting effect of the proposed scheme on Feeder1 is much less than that on Feeder2. However, the proposed scheme still has the feature of adaptive to fault positions.

TABLE V
ITBP OPERATION BEHAVIORS OF FEEDER2 AT DIFFERENT FAULT POSITIONS

Faulty line	Fault position	PSFC voltage (kV)			Tripping time (s)		
		$\lvert\Delta U_{13}'\rvert$	$\lvert\Delta U_{12}'\rvert$	$\lvert\Delta U_{11}'\rvert$	t_3	t_2	t_1
Line3	$x = 0$ km	8.814	5.770	3.226	0.504	1.000	1.424
	$x = 1$ km	8.143	5.326	2.974	0.603	1.074	1.466
	$x = 2$ km	7.533	4.906	2.740	0.705	1.144	1.505
	$x = 3$ km	6.996	4.554	2.549	0.795	1.203	1.537
	$x = 4$ km	6.545	4.254	2.378	0.870	1.253	1.566
	$x = 5$ km	6.117	3.985	2.227	0.941	1.297	1.591
Line2	Near-end		8.646	4.828		0.519	1.157
	Midpoint		6.926	3.867		0.806	1.317
	Far-end		5.775	3.224		0.999	1.425
Line1	Near-end			8.183			0.596
	Midpoint			6.062			0.951
	Far-end			4.827			1.157

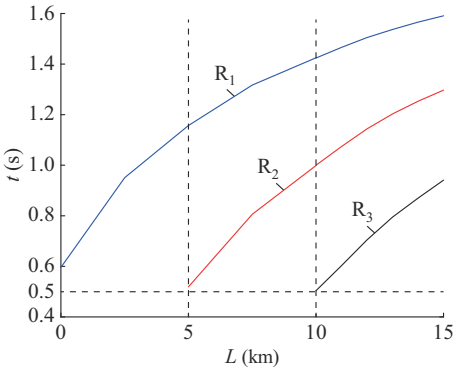

Fig. 10. Time-position coordination relationship of all relays obtained from Table V.

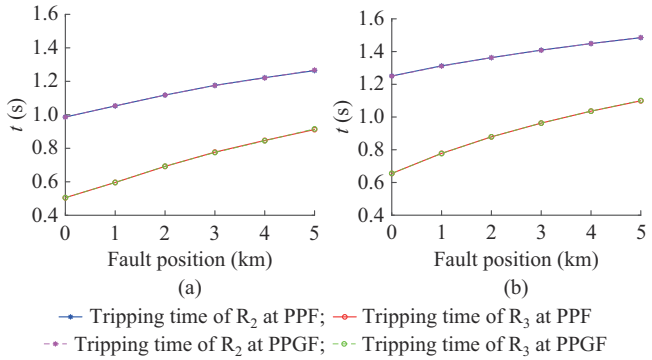

Fig. 11. Adaptation of proposed scheme to different fault types and feeders. (a) Fault occurs on Line3. (b) Fault occurs on Line5.

C. Simulation Verification with Fault Resistance

Figure 12 shows the effect of fault resistance R_g on protection performance, where Δt_{R23} is the tripping time difference between R_2 and R_3 in the case of a metallic fault. Compared

with a metallic fault, the PSFC voltage of each relay decreases when a fault via R_g and the PSFC voltage difference between adjacent upstream and downstream protections decreases. The tripping time of all relays increases and the time interval between adjacent protections decreases.

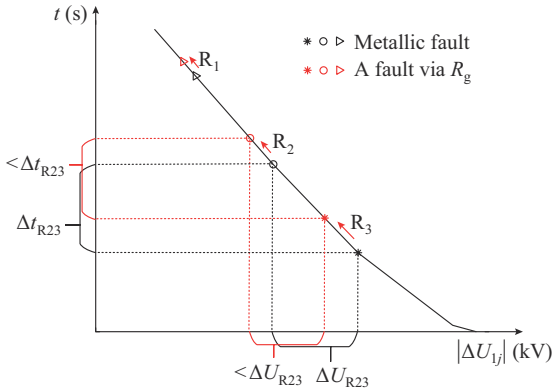

Fig. 12. Effect of fault resistance R_g on protection performance.

The "constraint value" in [3] can be used to evaluate the ability of ITBP to withstand the fault resistance. Assuming $c_{\Delta t_{23}}$ represents the constraint value for R_2 and R_3, and $c_{\Delta t_{12}}$ represents the constraint value for R_1 and R_2, we can obtain:

$$\begin{cases} c_{\Delta t_{23}} = t_2 - t_3 - CTI \\ c_{\Delta t_{12}} = t_1 - t_2 - CTI \end{cases} \tag{22}$$

When $c_{\Delta t_{23}}$ or $c_{\Delta t_{12}}$ is 0, it indicates that the adjacent upstream and downstream protections just meet the selectivity requirements. It corresponds to the minimum value of the PSFC voltage difference and the maximum value of R_g. The minimum of the PSFC voltage difference obtained by (19) is $0.2/|k_{13}|$. The value of k_{13} varies in different topologies and its corresponding maximum fault resistance is also different.

Table VI shows the ITBP operation behaviors when Line3 has a three-phase short-circuit fault via different fault resistance. Figure 13 shows the constraint values corresponding to Table VI.

TABLE VI
ITBP OPERATION BEHAVIORS WHEN LINE3 HAS A THREE-PHASE SHORT-CIRCUIT FAULT VIA DIFFERENT FAULT RESISTANCE

R_g (Ω)	Fault position	PSFC voltage (kV)			Tripping time (s)		
		$\|\Delta U'_{13}\|$	$\|\Delta U'_{12}\|$	$\|\Delta U'_{11}\|$	t_3	t_2	t_1
1	Near-end	8.091	5.325	2.978	0.612	1.074	1.466
	Midpoint	6.738	4.413	2.468	0.838	1.226	1.551
	Far-end	5.726	3.746	2.097	1.007	1.337	1.613
2	Near-end	7.435	4.927	2.749	0.721	1.140	1.504
	Midpoint	6.265	4.121	2.304	0.917	1.275	1.578
	Far-end	5.358	3.520	1.974	1.068	1.375	1.633
5	Near-end	5.667	3.775	2.108	1.017	1.333	1.611
	Midpoint	4.913	3.258	1.822	1.143	1.419	1.659
	Far-end	4.280	2.832	1.587	1.248	1.490	1.698

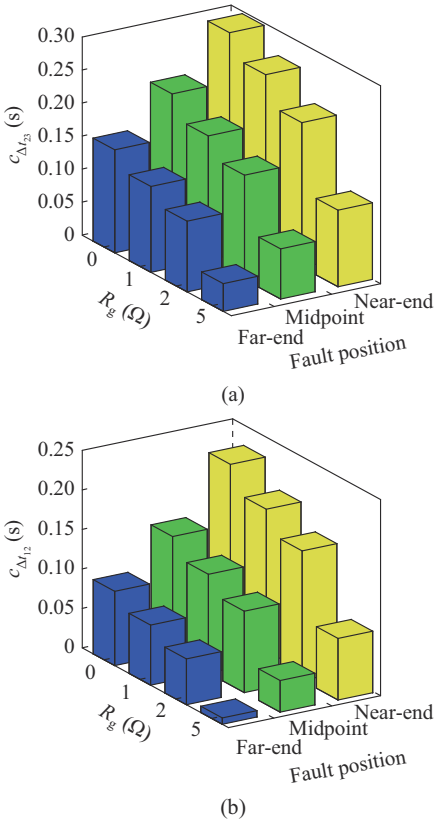

Fig. 13. Constraint values corresponding to Table VI. (a) $c_{\Delta t_{23}}$ (b) $c_{\Delta t_{12}}$.

It is known from (21) that the minimum PSFC voltage difference at the maximum fault resistance is 1.198 kV. As the fault resistance increases, the constraint value of adjacent protections decreases gradually, and its influence on the far-end fault is greater than that of the near-end fault. When the fault occurs at the far-end of Line3 and $R_g = 5\,\Omega$, $c_{\Delta t_{23}}$ and $c_{\Delta t_{12}}$ are greater than 0. Therefore, for multi-level coordinated relays, the proposed scheme has certain fault tolerant ability.

D. Adaptability Analysis for Different Line Lengths

When the line lengths in the network are different, especially when the lengths of two adjacent lines differ significantly, the range of upstream zone II distance protection will overlap with that of zone II distance protection of adjacent downstream, resulting in the loss of selectivity of backup protection [6]. The proposed ITBP scheme uses the near- and far-end faults of multiple specified points to calculate *TDS*, which considers the influence of line length on protection performance. However, when one of the two adjacent lines is much longer than the other, the PSFC voltage difference between adjacent protections will be significantly reduced. TDS_{max} increases significantly, resulting in a significant increase in the tripping time of all relays.

When the length of Line2 is 1 km, the corresponding tripping time curves are shown in Fig. 14. It can be observed that the tripping time of the ITBP tripping curve is much shorter than that of TDS_{max} but much longer than that of TDS_1. The right side of $y = |\Delta U_{12n}|$ is the protection range when ITBP is used as a near backup, which is not limited

by mutual coordination. Point q is the intersection of $y=0.14\cdot TDS_1/((\Delta U_j'^{*})^{0.02}-1)$ and $y=|\Delta U_{12n}|$. Therefore, the rapidity of protection is improved by translating the ITBP tripping curve down to the point q. It can be observed that the final tripping curve greatly reduces the tripping time of all relays. The translation method does not change the slope of the curve and therefore does not affect the coordination relationship between adjacent upstream and downstream protections.

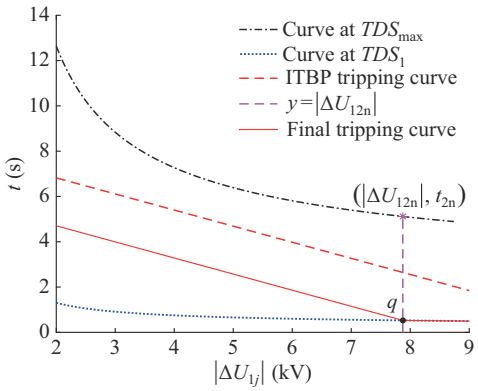

Fig. 14. Tripping time curves when length of Line2 is 1 km.

E. Adaptability Analysis of System Reconfiguration

Load transfer after a failure belongs to system reconfiguration [35]. The adaptability of the proposed scheme is analyzed when the left side of Line1 is disconnected from the system source S and the tie switch S_1 is closed. Compared with the original network, R_3 becomes a backup of R_2. Table VII shows the PSFC voltage and tripping time of three-level coordinated relays when DGs are connected and different fault types occur at the midpoint of Line1.

TABLE VII
PSFC Voltage and Tripping Time of Three-level Coordinated Relays

Fault type	PSFC voltage (kV)			Tripping time (s)		
	$\|\Delta U_{12}'\|$	$\|\Delta U_{13}'\|$	$\|\Delta U_{15}'\|$	t_2	t_3	t_5
Three-phase	8.190	5.974	2.629	0.595	0.965	1.266
PPF	8.341	6.206	2.911	0.570	0.927	1.230
PPGF	8.327	6.198	2.916	0.572	0.928	1.230

As shown in Table VII, the distribution pattern of the PSFC voltage still has the characteristic of being closer to the fault point and having a larger value. The tripping time calculated from (21) reflects the relative position of the relay in relation to the fault point. Thus, the proposed scheme can adapt to topology changes without the need for switching settings.

F. Performance Comparison of Different Protection Principles

For a high percentage of DGs connected to the grid, the ITBP and ITOC protection are used as backup protections, and their performance in realizing action sequence is compared. The parameter settings of the two protections are shown in Table VIII. The pickup current I_{pj} is predetermined based on the maximum load current.

TABLE VIII
Parameter Settings of ITBP and ITOC Protection

Relay	ITOC protection		ITBP			
	I_{pj} (kA)	TDS_j	ΔU_p (kV)	k_{13}	b_{13}	TDS_1
R_3	0.12	0.20				
R_2	0.23	0.23	0.77	–0.167	1.963	0.18
R_1	0.35	0.29				

Different cases of DG penetration are tested. The state without DG is called case 1, the state with DG connected to bus B is called case 2, and the state with DGs connected to buses B and C is called case 3. Figure 15 shows the fault current and PSFC voltage for each relay in the event of a three-phase metallic fault at the midpoint of Line3. Figure 16 shows the constraint values for the corresponding cases.

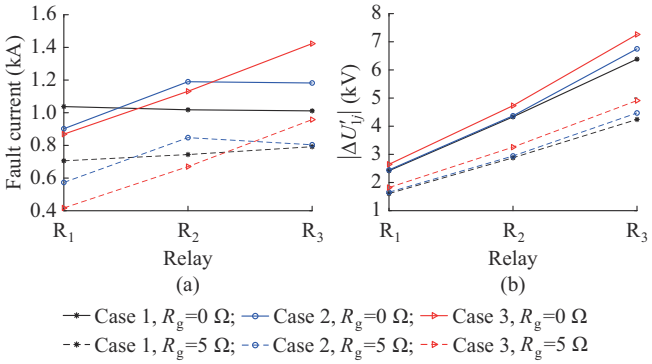

Fig. 15. Fault current and PSFC voltage for each relay in event of a three-phase metallic fault at midpoint of Line3. (a) Fault current. (b) PSFC voltage.

From Fig. 15, it can be observed that the distribution pattern of the fault current in the three cases is different and does not always satisfy the natural distribution rule, while the PSFC voltage always has a natural distribution pattern. Therefore, DG penetration has impact on the distribution pattern of the fault current, but not on that of the PSFC voltage.

As can be observed from Fig. 16, for a fault with $R_g=0\ \Omega$, the constraint value $c_{\Delta t_{12}}$ calculated by the proposed ITBP scheme for the three cases is smaller than that of the ITOC protection; for a fault with $R_g=5\ \Omega$, $c_{\Delta t_{23}}$ and $c_{\Delta t_{12}}$ calculated by the ITBP scheme for the three cases are smaller than those of the ITOC protection (especially $c_{\Delta t_{12}}$). These indicate that the proposed ITBP scheme has better rapidity when realizing the coordination of multi-level relays.

Although $c_{\Delta t_{23}}$ calculated by the proposed ITBP scheme is greater than that of the ITOC protection for case 2 with $R_g=0\ \Omega$, a comparison in case 1 shows that the proposed ITBP scheme is more adaptive to different DG connection locations and capacities. Therefore, the action performance of the proposed ITBP scheme is better than that of the ITOC protection when realizing adaptive coordination of multi-level relays.

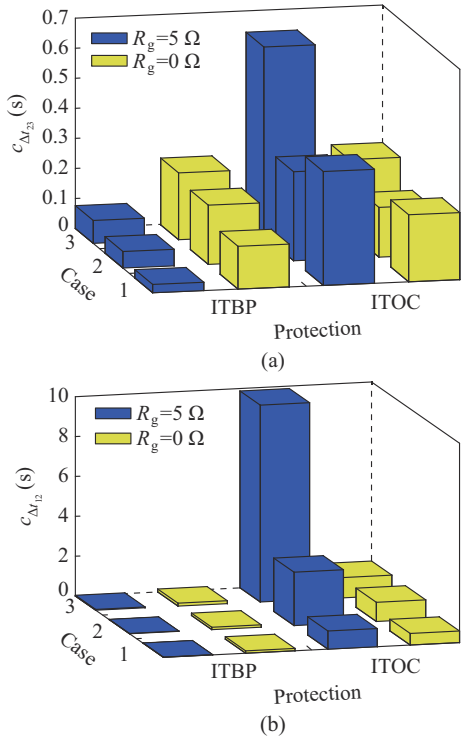

Fig. 16. Constraint values for different cases. (a) $c_{\Delta t_{23}}$. (b) $c_{\Delta t_{12}}$.

Table IX shows their comparative analysis in four aspects, including electrical quantity, distribution pattern, tripping time, and setting.

TABLE IX
COMPARATIVE ANALYSIS OF TWO PROTECTIONS

Protection	Electrical quantity	Distribution pattern	Tripping time	Setting
ITOC	Current	Affected by number and location of DGs	Long	With step-by-step setting whether there is DG or not
ITBP	Voltage	Not affected by number and location of DGs	Short	Without step-by-step setting

VI. CONCLUSION

The ITBP scheme based on the unified characteristic equation does not need to be set step-by-step. Adaptive coordination of adjacent upstream and downstream relays can be achieved without communication and using only PSFC voltage whose distribution pattern is not affected by DGs. Compared with the conventional scheme, the proposed ITBP scheme can be applied to distribution networks with high proportion of DGs. In addition, the proposed scheme is applicable to other network topologies where the PSFC voltage satisfies the natural distribution pattern. However, though combining the offline states of DGs to obtain a unified *TDS* for the whole network is easy to implement in radial networks, there are so many combined states of DGs in complex networks that *TDS* cannot be easily obtained. Therefore, in the following research, the key factors affecting the protection selectivity and sensitivity in complex topologies will be studied to realize the adaptive setting of inverse-time parameters.

REFERENCES

[1] M. Ezzeddine, R. Kaczmarek, and M. U. Iftikhar, "Coordination of directional overcurrent relays using a novel method to select their settings," *IET Generation, Transmission & Distribution*, vol. 5, no. 7, pp. 743-750, Jul. 2011.
[2] P. E. Muñoz, R. J. Mantz, and S. A. González, "Control-based fault current limiter for minimizing impact of distributed generation units on protection systems," *Journal of Modern Power Systems and Clean Energy*, vol. 11, no. 2, pp. 643-650, Mar. 2023.
[3] A. S. Noghabi, J. Sadeh, and H. R. Mashhadi, "Considering different network topologies in optimal overcurrent relay coordination using a hybrid GA," *IEEE Transactions on Power Delivery*, vol. 24, no. 4, pp. 1857-1863, Oct. 2009.
[4] N. Liu, J. Zhang, and W. Liu, "Toward key management for communications of wide area primary and backup protection," *IEEE Transactions on Power Delivery*, vol. 25, no. 3, pp. 2030-2032, Jul. 2010.
[5] E. Sorrentino, O. Salazar, and D. Chavez, "Limit curves by power system's transient stability for the inverse-time overcurrent relays," *IEEE Transactions on Power Delivery*, vol. 26, no. 3, pp. 1727-1733, Jul. 2011.
[6] J. Huang, Z. Li, Y. Zhang *et al.*, "Setting optimization of improved impedance correction inverse time overcurrent protection considering backup protection optimization series," *Power System Technology*, vol. 46, no. 7, pp. 2768-2777, Jul. 2022.
[7] H. Samet, T. Ghanbari, M. A. Jarrahi *et al.*, "Efficient current-based directional relay algorithm," *IEEE Systems Journal*, vol. 13, no. 2, pp. 1262-1272, Jun. 2019.
[8] V. C. Nikolaidis, E. Papanikolaou, and A. S. Safigianni, "A communication-assisted overcurrent protection scheme for radial distribution systems with distributed generation," *IEEE Transactions on Smart Grid*, vol. 7, no. 1, pp. 114-123, Jan. 2016.
[9] B. Anudeep and P. K. Nayak, "Differential power based selective phase tripping for fault-resilient microgrid," *Journal of Modern Power Systems and Clean Energy*, vol. 10, no. 2, pp. 459-470, Mar. 2022.
[10] N. Rezaei, M. N. Uddin, I. K. Amin *et al.*, "Genetic algorithm-based optimization of overcurrent relay coordination for improved protection of DFIG operated wind farms," *IEEE Transactions on Industry Applications*, vol. 55, no. 6, pp. 5727-5736, Dec. 2019.
[11] M. M. Mansour, S. F. Mekhamer, and N. El-Kharbawe, "A modified particle swarm optimizer for the coordination of directional overcurrent relays," *IEEE Transactions on Power Delivery*, vol. 22, no. 3, pp. 1400-1410, Jul. 2007.
[12] T. Amraee, "Coordination of directional overcurrent relays using seeker algorithm," *IEEE Transactions on Power Delivery*, vol. 27, no. 3, pp. 1415-1422, Jul. 2012.
[13] S. Stp, P. P. Verma, and K. S. Swarup, "A novel convexified linear program for coordination of directional overcurrent relays," *IEEE Transactions on Power Delivery*, vol. 34, no. 2, pp. 769-772, Apr. 2019.
[14] S. T. P. Srinivas and K. S. Swarup, "A new mixed integer linear programming formulation for protection relay coordination using disjunctive inequalities," *IEEE Power and Energy Technology Systems Journal*, vol. 6, no. 2, pp. 104-112, Jun. 2019.
[15] V. A. Papaspiliotopoulos, G. N. Korres, and N. G. Maratos, "A novel quadratically constrained quadratic programming method for optimal coordination of directional overcurrent relays," *IEEE Transactions on Power Delivery*, vol. 32, no. 1, pp. 3-10, Feb. 2017.
[16] K. A. Saleh, H. H. Zeineldin, A. Al-Hinai *et al.*, "Optimal coordination of directional overcurrent relays using a new time-current-voltage characteristic," *IEEE Transactions on Power Delivery*, vol. 30, no. 2, pp. 537-544, Apr. 2015.
[17] W. T. El-Sayed, M. A. Azzouz, H. H. Zeineldin *et al.*, "A harmonic time-current-voltage directional relay for optimal protection coordination of inverter-based islanded microgrids," *IEEE Transactions on Smart Grid*, vol. 12, no. 3, pp. 1904-1917, May 2021.
[18] S. Xu, Y. Lu, and Y. Wang, "A section voltage based inverse timing protection method for microgrid," *Automation of Electric Power Systems*, vol. 38, no. 1, pp. 68-73, Jan. 2014.
[19] S. Jamali and H. Borhani-Bahabadi, "Protection method for radial distribution systems with DG using local voltage measurements," *IEEE Transactions on Power Delivery*, vol. 34, no. 2, pp. 651-660, Apr. 2019.

[20] *IEEE Guide for Protective Relay Applications to Distribution Lines*, C37.230-2007, 2008, pp. 1-11.
[21] H. M. Sharaf, H. H. Zeineldin, D. K. Ibrahim *et al.*, "A proposed coordination strategy for meshed distribution systems with DG considering user-defined characteristics of directional inverse time overcurrent relays," *International Journal of Power and Energy Systems*, vol. 65, pp. 49-58, Feb. 2015.
[22] M. Ojaghi and R. Ghahremani, "Piece-wise linear characteristic for coordinating numerical overcurrent relays," *IEEE Transactions on Power Delivery*, vol. 32, no. 1, pp. 145-151, Feb. 2017.
[23] Z. He, Z. Zhang, W. Chen *et al.*, "Wide-area backup protection algorithm based on fault component voltage distribution," *IEEE Transactions on Power Delivery*, vol. 26, no. 4, pp. 2752-2760, Oct. 2011.
[24] N. Chang, G. Song, J. Hou *et al.*, "Fault identification method based on unified inverse-time characteristic equation for distribution network," *International Journal of Power and Energy Systems*, vol. 146, pp. 1-11, Mar. 2023.
[25] H. Gao, J. Li, and B. Xu, "Principle and implementation of current differential protection in distribution networks with high penetration of DGs," *IEEE Transactions on Power Delivery*, vol. 32, no. 1, pp. 565-574, Feb. 2017.
[26] *Technical Specification for Connecting Wind Farm to Power System – Part 1: Onshore Wind Power*, GB/T 19963.1-2021, 2021.
[27] Y. Li, Z. Wang, W. Wang *et al.*, "Impact and countermeasures of PV access distribution network with LVRT capability on reclosing," *Power System Protection and Control*, vol. 44, no. 15, pp. 61-67, Aug. 2016.
[28] M. E. Baran and I. El-Markaby, "Fault analysis on distribution feeders with distributed generators," *IEEE Transactions on Power Systems*, vol. 20, no. 4, pp. 1757-1764, Nov. 2005.
[29] X. Kong, Z. Zhang, X. Yin *et al.*, "Study on fault current characteristics and fault analysis method of power grid with inverter interfaced distributed generation," *Proceedings of the CSEE*, vol. 33, no. 34, pp. 65-74, Dec. 2013.
[30] F. Zhang and L. Mu, "A Fault detection method of microgrids with grid-connected inverter interfaced distributed generators based on the PQ control strategy," *IEEE Transactions on Smart Grid*, vol. 10, no. 5, pp. 4816-4826, Sept. 2019.
[31] L. Jiang, B. Liu, and S. Duan, "Supporting effect of power injection from distributed generations on voltage at grid-connected point during symmetrical short-circuit faults in power system," *Power System Technology*, vol. 38, no. 3, pp. 669-674, Mar. 2014.
[32] *Single Input Energizing Quantity Measuring Relays with Dependent or Independent Time*, GB/T 14598.7-1995, 1996.
[33] Y. Ge, *Principle and Technology of New Relay Protection and Fault Location*. Xi'an: Xi'an Jiaotong University Press, 2007, pp. 32-34.
[34] Z. Yuan, Q. Xu, G. Xu *et al.*, "Current protection optimization scheme in distribution network with large capacity distributed generators," *Power System Technology*, vol. 45, no. 5, pp. 1862-1868, May 2021.
[35] F. Friend, G. Johnson, B. Mugalian *et al*., "Effect of distribution automation on protective relaying," in *Proceedings of 2014 67th Annual Conference for Protective Relay Engineers*, College Station, USA, Mar. 2014, pp. 193-228.

Nana Chang received the B.S. degree in electrical engineering from Xi'an University of Technology, Xi'an, China, in 2012, and the M.S. degree in electrical engineering from North China Electric Power University, Beijing, China, in 2015. She is currently pursuing the Ph. D. degree in electrical engineering at Xi'an Jiaotong University, Xi'an, China. Her research interest includes fault identification in AC/DC distribution network.

Guobing Song received the Ph.D. degree in electrical engineering from the Xi'an Jiaotong University, Xi'an, China, in 2005. He is currently a Professor in the School of Electrical Engineering, Xi'an Jiaotong University. He is the Chairman of the DC Grid Protection Special Committee of IEEE PES (China) Power System Protection and Control Committee. His research interests include fault location, protection, and power electronics in power systems.

Zhongxue Chang received the B. S. degree in electrical engineering from Shanghai University of Electric Power, Shanghai, China, in 2013, and the M.S. and Ph.D. degrees in electrical engineering from Xi'an Jiaotong University, Xi'an, China, in 2020. He is currently an Assistant Professor from Xi'an Jiaotong University. His research interests include fault identification in AC/DC distribution network.

Yuping Zheng received the B.S. degree from Hefei University of Technology, Hefei, China, in 1983, the M. S. degree from Nanjing Automation Research Institute, Nanjing, China, in 1986, and the Ph.D. degree from Wuhan University, Wuhan, China, in 2004. He is currently working in the State Key Laboratory of Smart Grid Protection and Control, NARI Group Corporation, Nanjing, China. His research interests include relay protection and control of AC/DC hybrid power system.

Xingang Yang received the B. S. degree in electrical engineering from Xi'an Jiaotong University, Xi'an, China, in 2007. He is currently working at the Electric Power Research Institute of State Grid Shanghai Electric Power Company, Shanghai, China. His research interest includes renewable energy integration technology.